


 Cite this: *Chem. Commun.*, 2020, 56, 7511

 Received 13th March 2020,
 Accepted 28th May 2020

DOI: 10.1039/d0cc01926g

rsc.li/chemcomm

Unveiling the reaction mechanism of novel copper *N*-alkylated tetra-azacyclophanes with outstanding superoxide dismutase activity†

 Álvaro Martínez-Camarena,^a Pedro A. Sánchez-Murcia,^b Salvador Blasco,^b Leticia González^{b,c} and Enrique García-España^b

Quantum chemical and multiscale calculations reveal the mechanistic pathway of two superoxide dismutase mimetic *N*-alkylated tetra-azacyclophane copper complexes with remarkable activity. The arrangement of the binding site afforded by the bulky alkyl substituents and the coordinated water molecule as a proton source play key roles in the reaction mechanism.

The use of O₂ in the metabolism of aerobic organisms is associated with the generation of toxic reactive oxygen species (ROS).¹ The imbalance between their production and clearance leads to oxidative stress, thereby associated with the possible development of diseases.² Since the superoxide anionic radical (O₂^{•−}) is the first ROS species formed in the O₂ reductive pathway, the removal of its metabolic excesses is crucial to avoid oxidative stress. To do so, living organisms are equipped with superoxide dismutase enzymes (SODs), which transform O₂^{•−} into molecular oxygen (O₂) and hydrogen peroxide (H₂O₂).³ Inspired by nature, many efforts have been carried out to mimic the SOD activity with small molecules.⁴ Previous studies showed that polyazacyclophane receptors are capable of binding free metal ions, preventing ROS production and having protective capacity against ROS.^{1,4c,5} However, to the best of our knowledge, no compound has been approved yet for therapeutic intervention.^{4b}

With the aim to build up improved human SOD (hSOD) mimetics, we recently reported⁶ the design and synthesis of complex [CuL1(OH₂)]²⁺ **1** (Fig. 1A and B). In **1**, Cu²⁺ is complexed in the equatorial plane by the two nitrogen atoms of L1

(Fig. 1B) alkylated with isopropyl groups, by the pyridine nitrogen and by a water molecule, while the axial position is occupied by the methyl-alkylated nitrogen placed at the middle of the polyamine bridge of L1.⁷ Complex **1** shares with the active site of Cu in human SOD1 and SOD3 (hSOD1/hSOD3, in Fig. 1C) the fact that its coordination sphere is composed by four N-donors and a water molecule. Moreover, the crystallographic structure of **1** matches very nicely the square-pyramidal geometry of the electroactive site of the enzyme (Fig. 1D).

Here we report the *in vitro* SOD activity of **1** and unveil one of the first ever reported all-atom catalytic mechanisms for SOD mimetics. Using quantum mechanics (QM) and hybrid quantum chemistry molecular mechanics (QM/MM) methods we

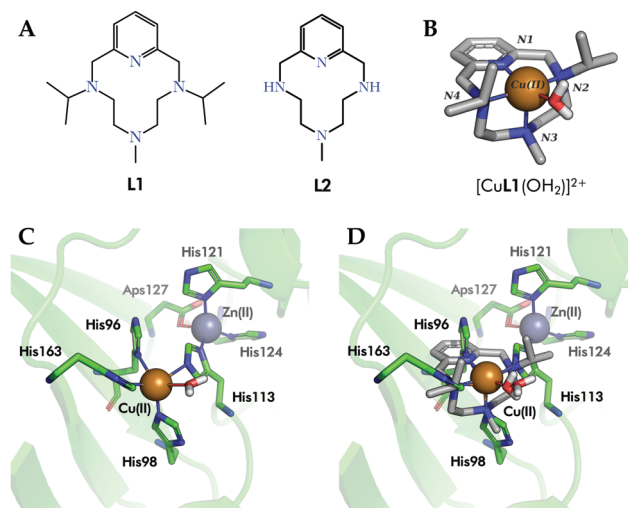


Fig. 1 (A) Ligands **L1** and **L2** are the macrocycle in complexes **1** and **2**, respectively. (B) Crystal structure of complex [CuL1(OH₂)]²⁺ (**1**), CCDC id. 1827336. (C) Detail of the active center of hSOD1 (PDB id. 2JLP). (D) Superimposition of complex **1** (sticks, carbon atoms colored in grey) within the active site of hSOD1 (green, PDB id. 2JLP). Only the inner sphere residues have been shown for simplicity.

^a ICMol, Departamento de Química Inorgánica, University of Valencia, C/Catedrático José Beltrán 2, 46980, Paterna, Spain. E-mail: alvaro.martinez@uv.es

^b Institute of Theoretical Chemistry, Faculty of Chemistry, University of Vienna, Währinger Str. 17, A-1090 Vienna, Austria. E-mail: pedro.murcia@univie.ac.at

^c Vienna Research Platform for Accelerating Photoreaction Discovery, University of Vienna, Währinger Str. 17, 1090 Vienna, Austria

† Electronic supplementary information (ESI) available. CCDC 1982975. For ESI and crystallographic data in CIF or other electronic format see DOI: 10.1039/d0cc01926g



Table 1 Logarithm of the stability constants for the Cu^{2+} complexes of **L1**⁶ and **L2** determined in 0.15 M NaClO_4 at 298.1 K

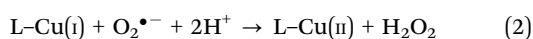
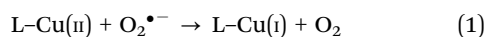
| Reaction ^a | $\log K$ (L1) | $\log K$ (L2) |
|--|------------------------|------------------------|
| $\text{Cu} + \text{L} \rightleftharpoons \text{CuL}$ | 14.04(1) ^b | 18.5(1) |
| $\text{CuL} + \text{H}_2\text{O} \rightleftharpoons \text{CuL(OH)} + \text{H}$ | -8.11(3) | -8.7(1) |

^a Charges omitted. ^b Values in parentheses are standard deviations in the last significant figure. Measurements were performed in triplicate.

show that, similar to the native SOD enzymes containing either Cu, Mn or Fe as electroactive metals, the coordinated water molecule plays a key role in the catalytic mechanism as a proton source and sink.

The *in vitro* SOD activity of **1** was measured at the physiological pH of 7.4 by means of the enzymatic assay developed by McCord–Fridovich.⁸ We also designed and tested complex $[\text{CuL2(OH}_2\text{)}]^{2+}$ (**2**) (see Fig. S10–S12, Table S1 and Table 1 with the potentiometric data in the ESI[†]), where the isopropyl substituents are absent (Fig. 1A). Although the bulkiness of the isopropyl substituents produces a slight decrease in the stability of the complexes,⁶ both ligands form very stable Cu^{2+} complexes at neutral pH. The SOD activities (k_{cat} values of $13.7 \times 10^6 \text{ M}^{-1} \text{ s}^{-1}$ for **1** and $7.2 \times 10^6 \text{ M}^{-1} \text{ s}^{-1}$ for **2**) are among the highest reported so far for synthetic SOD mimetics.⁹ Remarkably, the activities of **1** and **2** are only one order of magnitude below that of native hSOD1 ($43.0 \times 10^7 \text{ M}^{-1} \text{ s}^{-1}$).^{6,10} It is interesting to remark that the best performance is observed for the complex of the ligand with bulkier groups.

Encouraged by these results, we considered it of relevance to model the reaction mechanism of disproportionation of superoxide in the presence of copper complexes in order to identify the molecular features that govern the catalytic activity. Previous experimental kinetic studies showed that the disproportionation reaction is based on two elemental reactions:¹¹



The global reaction is very rapid and could reach the diffusion limit.¹² Theoretical studies of the superoxide disproportionation reaction mechanism catalysed by different isoforms of SODs^{12,13} support that the second half of the reaction is the time-limiting step and propose one of the chelating His residues (*e.g.* His113 in hSOD1, Fig. 1C) as a general acid agent to protonate the leaving peroxide. They also suggest that the residues of the surroundings affect the entrance and exit of the reactive species due to their electrostatic interactions. Thus, three different ways of binding the radical to the coordination sphere of the metal have been proposed so far: (i) the superoxide replaces one of the N/O binding sites, and therefore, some of the ligands or water molecules are removed from the coordination sphere, (ii) the superoxide binds Cu^{2+} increasing its coordination number from five to six, and (iii) the superoxide does not form any direct bond with copper and the electron transfer processes occur beyond the coordination sphere.^{12,13} The former three possibilities are known as dissociative, associative (inner sphere), and second-sphere mechanisms, respectively.^{13b}

Based on initial explorations, we assumed an associative mechanism as an initial hypothesis for both half-reactions (Fig. 2A), and we chose B3LYP-D3/def2-svp/Cu(MDF10) as level of theory (see Section IV in the ESI[†]) due to the good correlation between the obtained structures and the experimental ones. The solvent was implicitly treated with the polarizable continuum model. Fig. 2B shows the computed structures and energies of the catalytic cycle for **1**. Similar to SOD,¹⁴ it consists of two half-reactions (see also Fig. 2A): in the first one, Cu^{2+} is reduced to Cu^+ by oxidation of superoxide to molecular oxygen; in the second one, a new superoxide anion oxidizes Cu^+ to Cu^{2+} requiring two protons and releasing a molecule of hydrogen peroxide. In turn, each half-reaction may consist of three main steps: (i) the approach of the superoxide radical to the coordination sphere (π -complex **1-O}_2^{\bullet-}, intermediate **B**), (ii) the binding of $\text{O}_2^{\bullet-}$ within the copper coordination sphere (intermediates **A** or **D**), and finally, (iii) the leaving of products of the reaction (O_2 in complexes **A** or the peroxide in complexes **D**).**

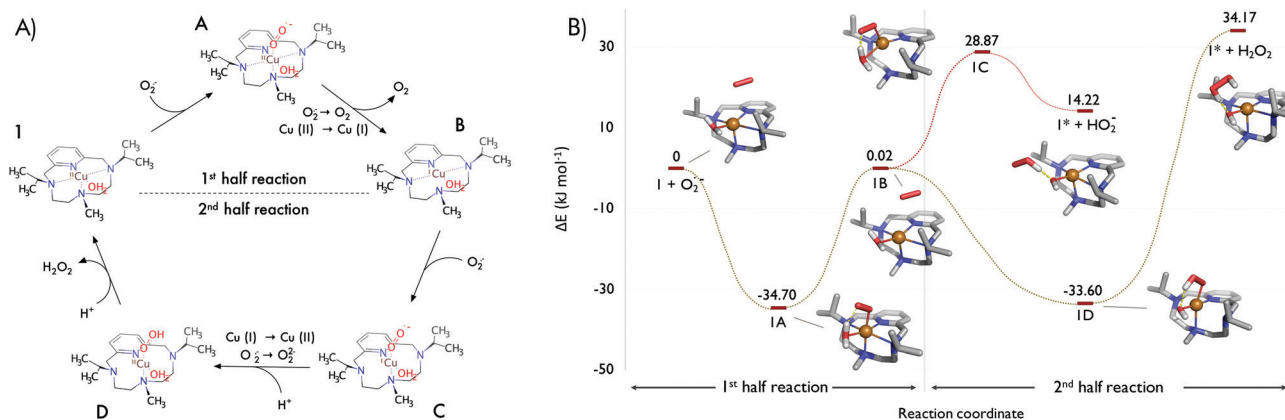


Fig. 2 (A) Proposed associative reaction mechanism for the catalysed disproportionation of superoxide by **1**: the oxidation of superoxide to O_2 (1st half reaction) and the reduction of a second molecule of superoxide to H_2O_2 (2nd half reaction). (B) Energy profile (kJ mol^{-1} , B3LYP-D3/def2-svp/Cu(MDF10), calculated in water using the SCRF method of the polarizable continuum model) for the reaction mechanism of the catalytic oxidation and reduction of two species of superoxide by complex **1**. Structure **1*** corresponds to the hydroxylated form of **1**.



In agreement with SOD enzymes,¹¹ our calculations predict that the first half-reaction is barrierless. No transition state was identified in the whole path (Fig. 2B). We also observed that the oxidation state of the metal centre strongly affects the geometry of the coordination sphere. In the first part of the reaction, the superoxide enters by forming a metastable π -complex that evolves into the intermediate **1A** in a process that releases energy (34.70 kJ mol⁻¹). The expansion of the coordination number of Cu²⁺ from 5 to 6 in **1A** corroborates that the first half reaction seems to follow an associative mechanism. Hexacoordinated intermediate **1A** has a distorted octahedral molecular geometry with the N2 and N4 (recall labelling in Fig. 1B) atoms in the axial positions. Remarkably, the superoxide enters into the coordination sphere by establishment of a hydrogen bond with the coordinated water molecule, which stabilizes **1A** in energy over 10 kJ mol⁻¹ (data not shown).

In the second half-reaction, the entering superoxide is reduced to hydrogen peroxide (Fig. 2A). Therefore, here the two protons should be provided by water molecules as no other ionizable groups are available in the surroundings. In order to select extra water molecules, we run QM/MM-MD simulations with complex **1B** (oxidation state Cu⁺ in the presence of a superoxide molecule and embedded in a box of water molecules, see Materials and methods). After a few picoseconds of simulation, the superoxide coordinates the metal centre from the face defined by the pyridine ring and opposite to the coordinated water molecule to form the associative intermediate **1C** (Fig. 2B). In such a disposition, the other oxygen of the superoxide is hydrogen-bonded to the coordinated water molecule and thus the first protonation is mediated by the coordinated water molecule (**1D**). The energy gap between **1C** and **1D** suggests that the entrance of the superoxide may be assisted by the proton transfer step. In addition, since the release of the monoprotinated peroxide is favourable (complex **1*** + HO₂⁻), the second protonation may also occur with the peroxide within the coordination sphere. Thus, the first protonation may follow an associative mechanism, with the coordinated water molecule as the general acid species to form the hydroxo intermediate **1D**. The finding of a hydroxo intermediate is supported by the crystal structure of *E. coli* Mn-SOD (PDB id. 1IX9 and 1IXB) in which the Mn³⁺ is postulated to be bound to a hydroxo ligand.¹⁵ Previous QM computational studies of Fe^{-13a} and Mn-SODs¹³ support the idea that the relevant forms of Fe³⁺-SOD and Mn³⁺-SOD are the hydroxo intermediates.⁷

The second protonation step to generate the hydrogen peroxide from **1D** must involve a second water molecule from the solvent, in contrast to hSOD1, where the leaving of the peroxide is preceded by its protonation by a His residue to yield H₂O₂.^{12,16} It must be stressed that the second protonation is a highly endothermic step in our calculations (>60 kJ mol⁻¹). Since the catalyst requires a third protonation to be regenerated into complex **1**, this final protonation may occur before or together with the release of H₂O₂. Therefore, the coordinated water molecule (or its hydroxo counterpart) plays a pivotal role in the entering and leaving of the substrate.

In order to prove that the coordinated water molecule does not leave the coordination sphere and acts as a general acid,

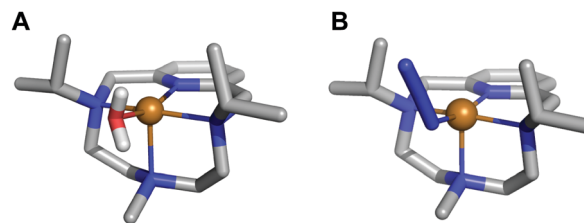


Fig. 3 (A) Crystal structure of complex [CuL1(OH₂)]²⁺ (**1**), CCDC id. 1827336. (B) Crystal structure of complex [CuL1(N₃)]⁺, CCDC id. 1982975.

1 was reacted with NaN₃ to replace the coordinated water molecule by N₃⁻ before running the catalytic reaction. The determination of the interaction constant of N₃⁻ with [CuL1(OH₂)]²⁺ confirmed its capacity to occupy the fifth coordination position in the complex (log *K* = 3.05(1)), substituting the coordinated water as evidenced by the crystal structure in Fig. 3 and Fig. S13–S16 (ESI[†]). The measurements showed that the addition of NaN₃ to a solution of [CuL1(OH₂)]²⁺ leads to a 4-fold reduction of its catalytic constant from 13.7 × 10⁶ to 3.7 × 10⁶ M⁻¹ s⁻¹ (when 1:1:5 Cu²⁺:L:N₃⁻ molar ratio is used). These results support our hypothesis that the water molecule (or its hydroxo form) remains bound to Cu throughout the whole catalytic cycle and acts as a general acid. With N₃⁻ in the coordination sphere, there is no water bound to the metal centre, the proton has to be acquired from the first water shell and thereby the catalytic activity drops.

For the second half reaction, if we compare complexes **1C** (path not favourable) and **1D**, there are significant differences between their structures. In **1C**, L1 coordinates the copper atom just through N1 and N4, while in **1D** the L1 the chelating atoms are N1 and N3 (atoms N2 and N4 do not coordinate now the copper centre). Intermediate **1C** shows a highly distorted tetrahedral geometry ($\tau_4 = 0.61$), whereas intermediate **1D** presents a smaller τ_4 value (0.12), which can be related to a distorted square planar geometry ($\tau_4 = 0$ square planar; $\tau_4 = 1$ tetrahedral geometry).¹⁷ Thus, associated with the reduction of the superoxide radical in **1D**, there is a conformational change in the adduct that leads to a square planar geometry from a square-pyramid one (**1B**).

We also computed the energy profile of complex **2**, where the two isopropyl groups on nitrogens N2 and N4 were removed (Fig. S17, ESI[†]). **2** follows a similar trend as **1**. However, the intermediate **2A** in the first-half reaction is much more stabilized in energy than **1A**. Since this process is barrier-less and this step shows the lowest energy of the reaction, the kinetics should be governed by the relative energy of the former two intermediates. This can be rationalized by an over stabilization of the catalyst-substrate adduct in **2** by the formation of hydrogen bonds not only with the water molecule complexed to the copper, but also with the hydrogen atoms belonging to the secondary amines of L2 (see Fig. S18 in the ESI[†]). This explains why the turnover of the catalyst decreases,¹⁸ as escaping from this minimum costs more energy than in complex **1A**. This hypothesis is confirmed by the experimental measurements of the catalytic constant of **2**, which is half of the value of **1**. The second-half reaction in **2** is like that of **1**.



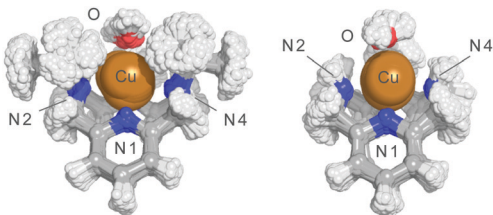


Fig. 4 Superimposition of structures of complexes **1** and **2** obtained along the QM/MM MD simulations.

Finally, we also analysed the dynamical behaviour of both complexes in aqueous solution by means of four QM/MM MD simulations considering both oxidation states (Cu^{2+} and Cu^+) in the presence or absence of a superoxide molecule (see the ESI^\dagger). In the absence of superoxide, the alkylation of N2 and N4 with isopropyl groups in **1** reduces the Cu–N2/N3/N4 bond order regardless of the oxidation state (Table S2, ESI^\dagger). This means that the Cu–N bonds are longer in **1** than that in **2**, with a broader distribution of the N–Cu bond distances along the simulations (the mean value for the Cu–N4 bond in **1** is 0.2 Å longer than that in **2**, with a broader distribution along the simulation). To a minor extent, the Cu–N2 and Cu–N3 distances also increase in **1**. Fig. 4 shows the superimposition of the structures obtained for each one of the complexes along the QM/MM MD trajectory. Furthermore, the evolution of the Cu–N2 distance for the complexes in their different oxidation states along the catalytic reaction mechanism is shown in Fig. S19 (ESI^\dagger). Clearly, in **2** the Cu–N2 bond order increases along all the catalytic cycle. The same feature is observed for the Cu–N3 and Cu–N4 bonds (Tables S6–S9, ESI^\dagger). These observations agree with the stability constants determined by the potentiometric titrations (Table 1). The reduction of four orders of magnitude of the Cu^{2+} complexation constant for **L1** with respect to **L2** is in agreement with the fact that its coordinative centre shows a broader distribution of bond distances and a higher average value. Thus, isopropylation of N2 and N4 in complex **1** increases the weakness of the N–Cu bonds and helps the complex to switch easily between the geometries implicated in the catalytic cycle, increasing the catalytic constant. The steric factors introduced by the isopropyl groups may also control the entrance of the superoxide to the coordination sphere by one face of the complex (Fig. S20, ESI^\dagger).

In summary, this work reports the *in vitro* SOD catalytic activities of two *N*-alkylated tetra-azacyclophane copper complexes with remarkable antioxidant activities. Their mode of action, transforming the two superoxide molecules into oxygen and hydrogen peroxide in a catalysed cycle is put forward for the first time. It is observed that the isopropylation of the nitrogen atoms of the azacyclophane ring facilitates the structural changes required along the catalytic cycle and helps to orientate

the entrance of the reactive species into the coordination sphere. Moreover, we confirm, both theoretically and experimentally, the key role of the coordinated water in the catalytic cycle of such SOD mimetics.

A. M.-C. thanks the Spanish Ministry of Science, Innovation and Universities for grants FPU14/05098 and EST16/00533. P. A. S.-M. and L. G. thank the University of Vienna, the Austrian FWF for financial support (Lise Meitner Project M 2260), and the Vienna Scientific Cluster (VSC3) for computational time. MINECO is acknowledged for the grants Juan de la Cierva (SB) and CTQ2016-78499-C6-1-R, CTQ2017-90852-REDC and Unidad de Excelencia María de Maeztu MDM-15-0538.

Conflicts of interest

There are no conflicts to declare.

Notes and references

- 1 K. M. Lincoln, P. Gonzalez, T. E. Richardson, D. A. Julovich, R. Saunders, J. W. Simpkins and K. N. Green, *Chem. Commun.*, 2013, **49**, 2712.
- 2 L. R. Perez and K. J. Franz, *Dalton Trans.*, 2010, **39**, 2177.
- 3 Y. Sheng, I. A. Abreu, D. E. Cabelli, M. J. Maroney, A. F. Miller, M. Teixeira and J. S. Valentine, *Chem. Rev.*, 2014, **114**, 3854.
- 4 (a) S. Gandhi and A. Y. Abramov, *Oxid. Med. Cell. Longevity*, 2012, **2012**, 11; (b) L. E. Scott and C. Orvig, *Chem. Rev.*, 2009, **109**, 4885; (c) A. Martínez-Camarena, E. Delgado-Pinar, C. Soriano, J. Alarcón, J. M. Llinares, R. Tejero and E. García-España, *Chem. Commun.*, 2018, **54**, 3871; (d) D. P. Riley, *Chem. Rev.*, 1999, **99**, 2573; (e) D. Salvemini, D. P. Riley and S. Cuzzocrea, *Nat. Rev. Drug Discovery*, 2002, **1**, 367.
- 5 D. E. Green, M. L. Bowen, L. E. Scott, T. Storr, M. Merkel, K. Böhmerle, K. H. Thompson, B. O. Patrick, H. J. Schugar and C. Orvig, *Dalton Trans.*, 2010, **39**, 1604.
- 6 Á. Martínez-Camarena, A. Liberato, E. Delgado-Pinar, A. G. Algarra, J. Pitarch-Jarque, J. M. Llinares, M. Á. Mañez, A. Domenech-Carbó, M. G. Basallote and E. García-España, *Inorg. Chem.*, 2018, **57**, 10961.
- 7 J. Azadmanesh and G. E. O. Borgstahl, *Antioxidants*, 2018, **7**, 25.
- 8 (a) C. Beauchamp and I. Fridovich, *Anal. Biochem.*, 1971, **44**, 276; (b) J. Y. Zhou and P. Prognon, *J. Pharm. Biomed. Anal.*, 2006, **40**, 1143.
- 9 (a) O. Iranzo, *Bioorg. Chem.*, 2011, **39**, 73; (b) I. Batinić-Haberle, J. S. Rebouças and I. Spasojević, *Redox-Active Therapeutics*, Springer, 2016.
- 10 H. Ohtsu, Y. Shimazaki, A. Odani, O. Yamauchi, W. Mori, S. Itoh and S. Fukuzumi, *J. Am. Chem. Soc.*, 2000, **122**, 5733.
- 11 (a) J. Rabani, D. Klug and I. Fridovich, *Isr. J. Chem.*, 1972, **10**, 1095; (b) D. Klug-Roth, J. Rabani and I. Fridovich, *J. Am. Chem. Soc.*, 1973, **95**, 2786.
- 12 M. Lintuluoto, C. Yamada and J. M. Lintuluoto, *J. Phys. Chem. B*, 2017, **121**, 7235.
- 13 (a) L. Rulišek, K. P. Jensen, K. Lundgren and U. Ryde, *J. Comput. Chem.*, 2006, **27**, 1398; (b) M. Srnc, F. Aquilante, U. Ryde and L. Rulišek, *J. Phys. Chem. B*, 2009, **113**, 6074.
- 14 P. J. Hart, M. M. Balbirnie, N. L. Ogihara, A. M. Nersissian, M. S. Weiss, J. S. Valentine and D. Eisenberg, *Biochemistry*, 1999, **38**, 2167.
- 15 I. A. Abreu and D. E. Cabelli, *Biochim. Biophys. Acta*, 2010, **1804**, 263.
- 16 D. Chen, Q. Wang, H. Zhang, S. Mi, J. Wang, Q. Zeng and G. Zhang, *Int. J. Quantum Chem.*, 2010, **110**, 1394.
- 17 L. Yang, D. R. Powell and R. P. Houser, *Dalton Trans.*, 2007, 955.
- 18 E. Sperotto, G. P. M. van Klink, J. G. de Vries and G. van Koten, *Tetrahedron*, 2010, **66**, 3478.

